Genesis of thunderstorm ground enhancements

A. Chilingarian, G. Hovsepyan, T. Karapetyan, D. Aslanyan, S. Chilingaryan, and B. Sargsyan
Yerevan Physics Institute, Alikhanyan Brothers 2, Yerevan, Armenia, 0036

(Received 30 January 2023; accepted 7 April 2023; published 9 May 2023)

Proceeding from a stormy day on 22 September 2022, when seven thunderstorm ground enhancements occurred (TGEs, three of them very large), we analyze closely the TGEs' energy spectra and conditions supporting the unleashing of the intense particle flux. For the first time, we present a detailed analysis of the shape of the TGE energy spectra in the energy range from 0.3 to 50 MeV and discuss the conditions of TGE origination. The cross calibration of different detectors is possible thanks to the 24/7 monitoring of particle fluxes with numerous detectors and spectrometers operated on Aragats cosmic ray observatory. Despite the difficulties of measuring energy spectra from an electron accelerator with a beam size of several km^2, which can change the electron energy in seconds, we reliably recover energy spectra of electrons and gamma rays. We estimate the intensity of the most significant particle flux to be $\approx 1,25$ million TGE particles with energies greater than 0.3 MeV hitting each square meter of surface on Aragats, 3200 asl. We analyze the charged structure of the thundercloud giving birth to the operation of the lower dipole, which accelerates electrons, and discuss the precursors of the lighting flashes.

DOI: 10.1103/PhysRevD.107.102003

I. INTRODUCTION

During thunderstorms, strong electric fields modulate the energy spectra of cosmic rays and cause short and long bursts. Large amplifications of particle fluxes, the so-called thunderstorm ground enhancements (TGEs, [1,2]) manifest themselves as prominent peaks in the time series of count rates of particle detectors. Intense fluxes of electrons and gamma rays, measured on mountain peaks, can exceed the background up to 200 times [3]. Relativistic electron runaway avalanches (RREAs) occur when the atmosphere's electric field strength exceeds the critical value for starting a relativistic electron runaway avalanche (RREA [4]), during which the free electrons multiply, accelerate, and form avalanches reaching the Earth's surface. Free electrons, abundant at any altitude in the atmosphere from extensive air showers (EASs), serve as seeds for atmospheric electron accelerators.

Measurements of the energy spectra of electrons and gamma rays on Aragats make it possible to identify emerging electrical structures in the atmosphere (lower dipole), which accelerate seed electrons to 50 MeV or more [5]. The accelerating dipole is formed by the main negatively (MN) charged layer in the middle of the cloud and its mirror on the Earth. Usually, during thunderstorms, an additional lower positively charged region (LPCR) emerges at the bottom of the cloud, also forming an accelerating dipole with MN [6]. This dipole was discovered by Joachim Kuettner on Zugspitze at the end of 40ths of the last century [7] and is related to falling positively charged graupel.

The time series of more than 300 TGEs registered on Aragats, of near-surface electric field (NSEF) and geomagnetic field, lightning location, and weather parameters are available from the Mendeley dataset [8]. A lightning flash abruptly terminates most TGEs on Aragats; see the dataset of 165 TGEs in [9].

The relation of electron fluxes to lightning initiation is one of the most challenging problems in atmospheric research. Precise experiments on Aragats give clues for understanding this relationship and establishing the time sequence of both [10]. Understanding high-energy processes in the atmospheric plasma will help research particle accelerators operating on much larger scales in the space plasmas.

The summer of 2022 (July–September on Aragats research station, 3200 m asl.) was dry and hot. The outside temperature was higher than usual, exceeding 15 °C half the time. In 3 months, there were only six thunderstorms, as shown in Fig. 1 by disturbances of the NSEF (blue time series in Fig. 1) and lightning flashes (green lines at the top). On the time series of the count rate of the particle detector (black time series), impulsive enhancements were minimal, suddenly enormously intensifying on 22 September, when three enormous particle flux enhancements were registered.

In Figs. 2(a)–2(c), we presented four episodes of TGE registration in the summer of 2022.

The particle flux enhancement during very few summer TGEs in 2023 stayed at most 8%. The corresponding significances measured in the number of standard deviations relative to fair weather value was at most 10%. Suddenly, on September 22, during an ordinary storm, in 5 hours, detectors registered three record enhancements, the largest of which at 9:20 demonstrated ≈150% enhancement

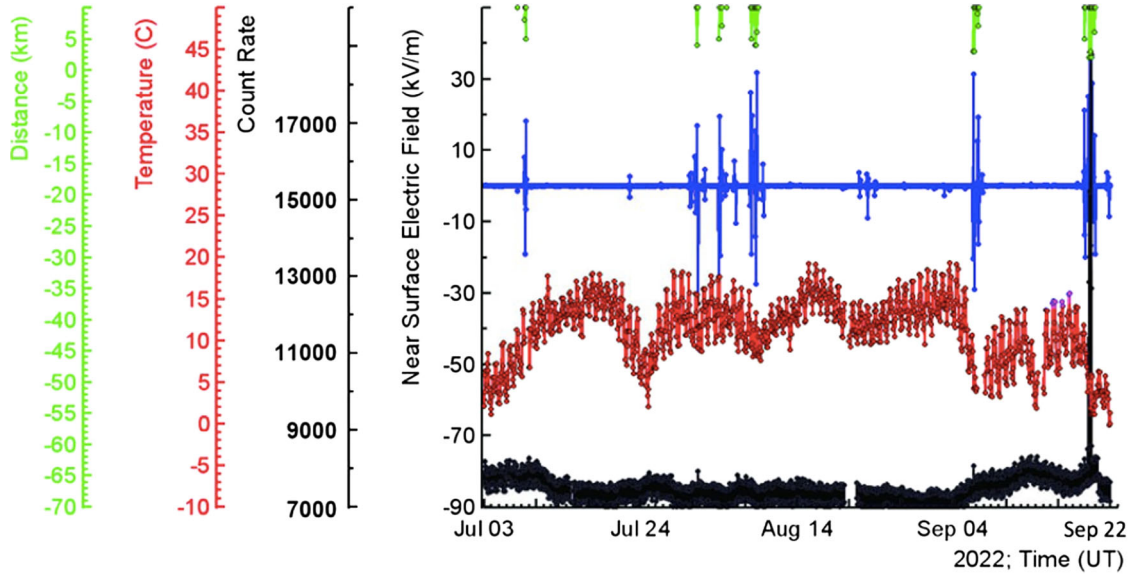

FIG. 1. Summer 2022: black—time series of 1-min count rates of STAND3 plastic scintillator of 1 m^2 area and 3 cm thickness; blue—disturbances of the NSEF measured by EFM 100 electric mills produced by the BOLTEK firm, widely used in atmospheric physics research; red—outside temperature; green—distances to lightning flashes.

in 1-mintime series of the upper from four vertically stacked STAND3 [11] detectors scintillators ["1000" coincidence, signal only in the upper scintillator, Fig. 2(d)]. To understand environments leading to such an enormous count rate surplus and to demonstrate paths of TGE physical analysis, we studied the 22 September events in all detail, performing all necessary reliability checks.

Among numerous particle detectors operated on Aragats, the most important is the Aragats solar neutron telescope (ASNT [12]), the only spectrometer that can resolve TGE particle mixture and estimate the energy spectra of electrons and gamma rays separately. We check the uniformity of operation of eight scintillators of ASNT, examining the background count rates before and after the TGE events.

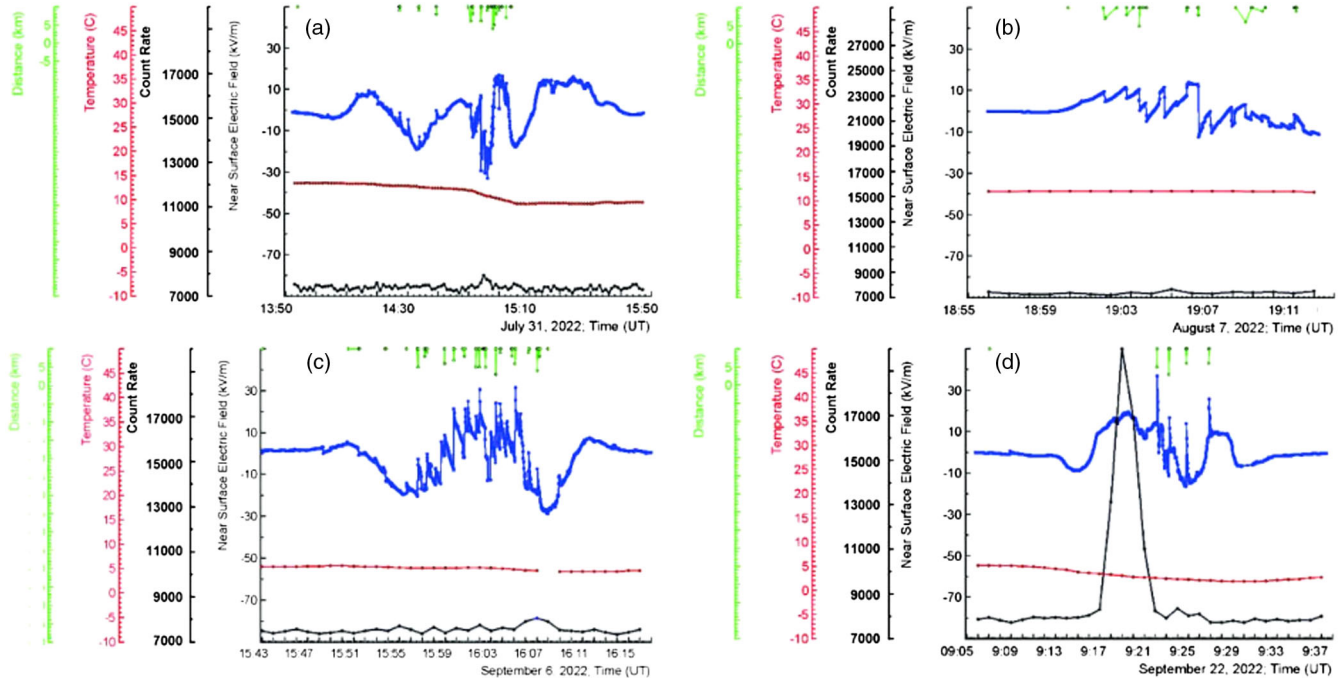

FIG. 2. TGE events occurred on Aragats from July to September 2022. The description of colored curves is the same as in Fig. 1.

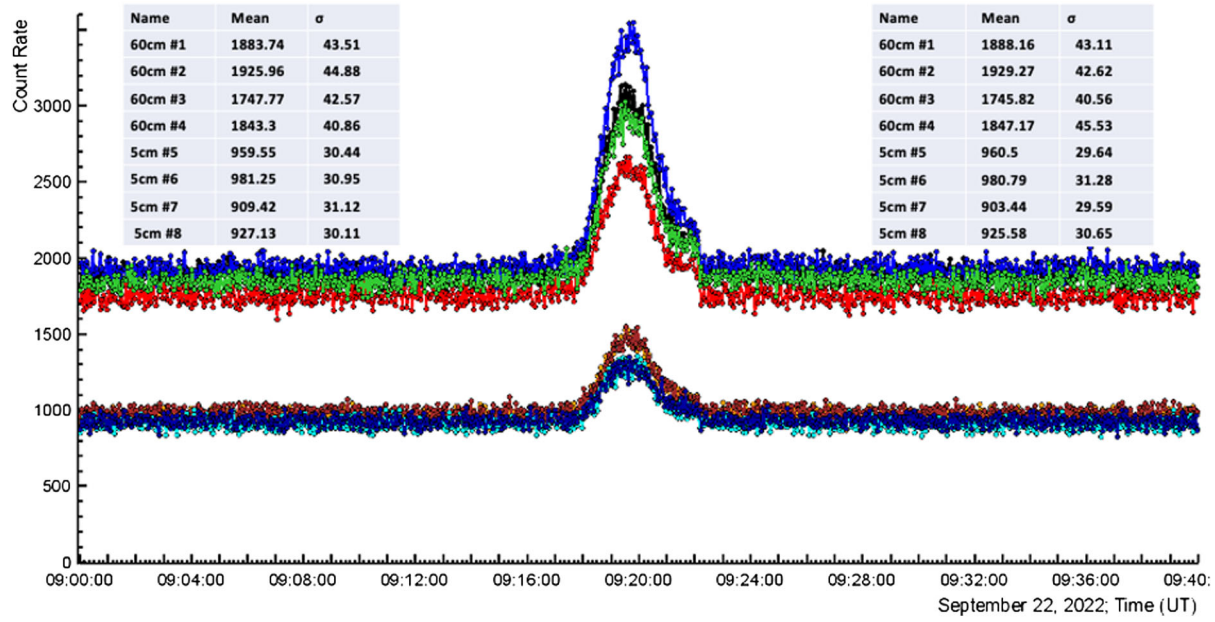

FIG. 3. 2 s time series of count rates of 8 ASNT scintillators (four 5 cm thick "veto" scintillators and four 60 cm thick spectrometric scintillators). The insets show mean values and variances of the count rates before and after TGE.

In Fig. 3, we demonstrate the variation of the count rates measured by eight scintillators, which comprises ≈10% for the 60 cm thick scintillators and ≈5% for the 5 cm thick ones. During TGE (with a large share of low energy particles), the difference between count rates is more prominent, reaching 30% for the second and third 60 cm thick scintillators (blue and red) due to slightly different energy thresholds. However, we present energy spectra only for energies above 10 MeV; thus, the difference between the count rates at low energies is unimportant.

A. The energy spectra recovering from the TGE event occurred at 9:20, 22 September 2022

In Fig. 4, we present the time series of count rates of the sum of four thick ASNT scintillators with different

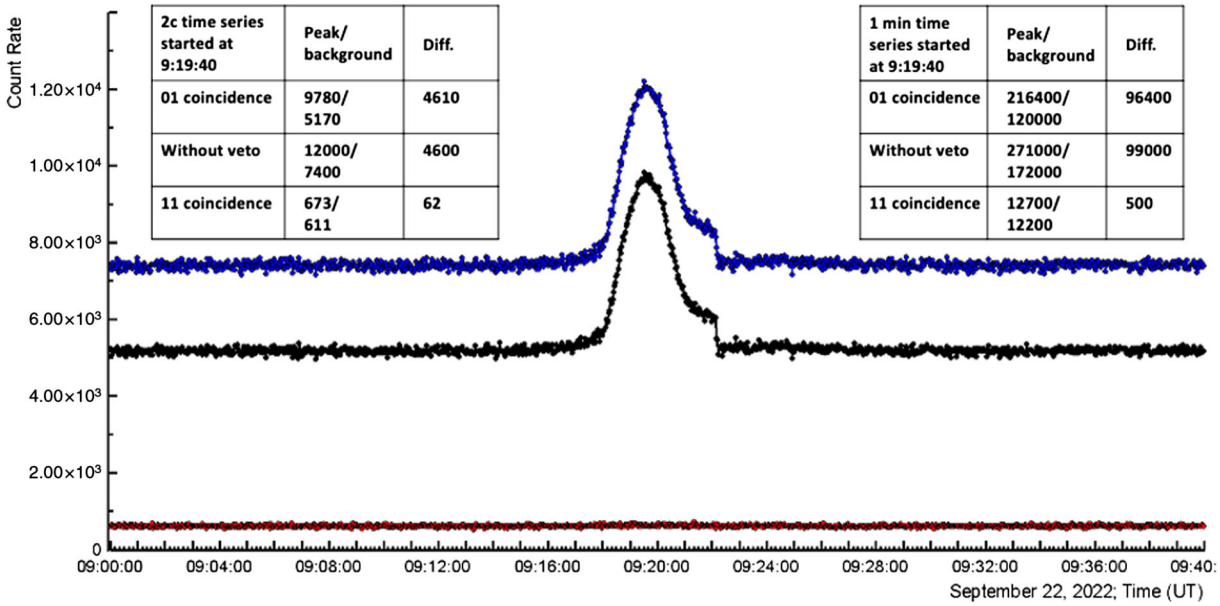

FIG. 4. 2 s time series of count rates of ASNT coincidences: "01", mainly gamma rays, black; "11", primarily electrons, red; and count rate of all particles registered in the lower 60 cm thick scintillator, blue. In the insets, the maximum flux and background (measured before TGE start) are shown; the difference of both (TGE flux) is calculated for the 2 s (left inset) and 1-min (right inset) count rates.

selection criteria. The "01" coincidence (signal only in the lower 60 cm thick scintillator) selects mainly gamma rays. The "11" coincidence (signal in both layers) picks electrons primarily.

TGE started at 9:17 when NSEF was near zero and smoothly rose with the enhancement of NSEF [Fig. 2(d)]. At the maximum of TGE flux at 9:19:30, NSEF reached 20 kV/m. Afterward, TGE coherently declined with the weakening of the NSEF until the normal polarity lightning flash abruptly terminated it at 9:22:10.

In Fig. 4, we see that the electron flux (red curve) was too small to be reliably recovered (see the left inset in Fig. 4, only 62 "11" coincidences were observed in 2 s). We summarize thirty 2 s counts to obtain a 1-min count rate (see the right inset of Fig. 4). In 1-min, we have 500 electron candidates (coincidence "11"); in turn, the number of gamma ray candidates is 96400 (coincidence "01"). Thus, it will not be easy to disentangle the ≈0.5% fraction during the energy recovery procedure. Nonetheless, we notice slight electron content in Fig. 5. Figure 5(a) shows the 1-min time series of "11" coincidence (signals in upper and lower scintillators). In Fig. 5(b), we offer the energy release histogram in a 5 cm thick upper scintillator of ASNT.

By the blue arrow, we point to a peak in the energy release distribution in a 5 cm thick scintillator. As electrons leave ≈1.8 MeV energy release due to ionization in every centimeter of the scintillator, we expect a peak from electrons in the 6–9 MeV interval. The distribution of the energy losses by gamma rays follows exponential law and exhibits no peaks. Thus, this minor deviation from the exponent is due to electrons in the TGE flux.

We also recover the TGE energy spectrum with the NaI spectrometer network operated on Mt. Aragats. Five large ($12 \times 12 \times 28$ cm) NaI (Tl) crystals are located under the roof of the SKL experimental hall on Aragats and have an energy threshold of 0.3 MeV (see details in [7]). For fitting TGE energy spectra, we use a five-parametric fit function, which was used to fit the primary cosmic ray spectrum measured by the MAKET ANI surface array [13,14].

$$dI/dN = A * E^{-\gamma_1}(1 + (E/E_{\text{knee}})^{\varepsilon})^{\Delta\gamma/\varepsilon},$$

energy spectra exhibit a "knee" feature (the spectrum turnover point) around 6–7 MeV, $\Delta\gamma = \gamma_1 - \gamma_2$ is the difference of spectral indexes before and after the knee, γ_1 varies from 1.27 to 1.33, γ_2—from −3.00 to 3.17, and the sharpness of the knee ε from 2.53 to 3.3.

Before the knee, the TGE gamma rays are contaminated by the intense radon progeny gamma radiation [15], making spectra relatively soft. At energies higher than 10 MeV spectra smoothly hardening, indices change from (1.27–1.31) to (2.81–3.17). TGE started at 9:18 and was terminated by a lightning flash at 9:21:10; thus, in the first and last minutes [Figs. 6(a) and 6(d)], intensities were weaker than at 9:19–9:20 [Figs. 6(b) and 6(c)]. At the maximum of TGE, 9:19–9:20, approximately 1,25 million TGE particles with energies above 0.3 MeV hit every square meter of the Earth's surface, covering several square kilometers on the ground; see Fig. 7.

In Fig. 8, we show the time series of the distance to the cloud base, estimated by the difference between surface temperature and dew point (the so-called spread). The blue arrow shows that during TGE, the cloud base height was ≈200 m. Assuming that the electric field is prolonged only in the cloud, the distance is too large, even for >40 MeV electrons, to reach the ground. If NSEF is positive, the MN layer is screened, and electrons accelerate and multiply in the dipole formed by the negatively charged MN layer in the middle of the cloud and transient positively charged region LPCR sitting on the falling graupel. The conical graupel fall (3–5 mm in size) can be noticed by shots of panoramic cameras monitoring skies above Aragats; see Fig. 9. The characteristic specks on the camera's glass are graupel; the station staff performed the graupel identification comparing the photos of specks and pictures of fallen conical graupel, see Figs. 11 and 12 in [16].

As we can see from the camera shots, the graupel fall starts just after the maximum TGE intensity and lasts 6 min. The MN and LPCR control the sign of the NSEF; the main positive charged layer on the top of the thundercloud only weakly influences the NSEF. The existence or absence of the LPCR is illustrated by the graupel fall, which usually exists in the lower thunderous atmosphere at surface temperature −3 °C– + 3 °C. When low and large,

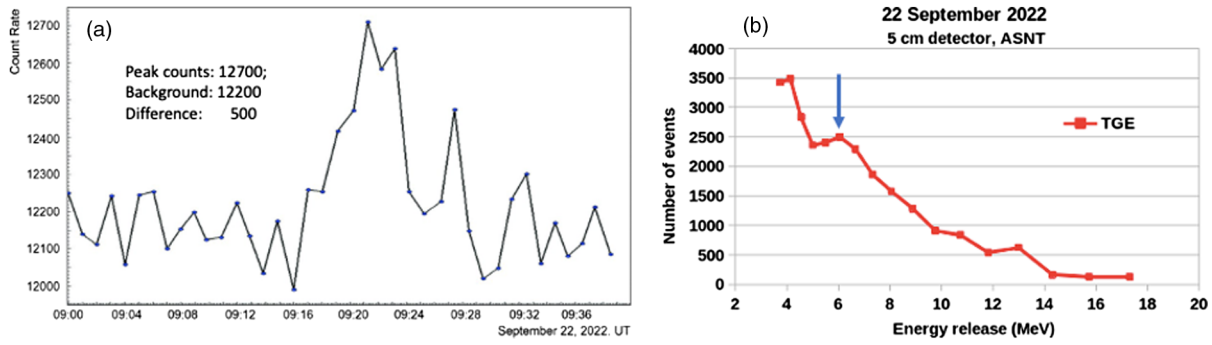

FIG. 5. (a) 1-min time series of the "11" coincidence; (b) the energy release histogram in the 5-cm thick upper scintillator of ASNT.

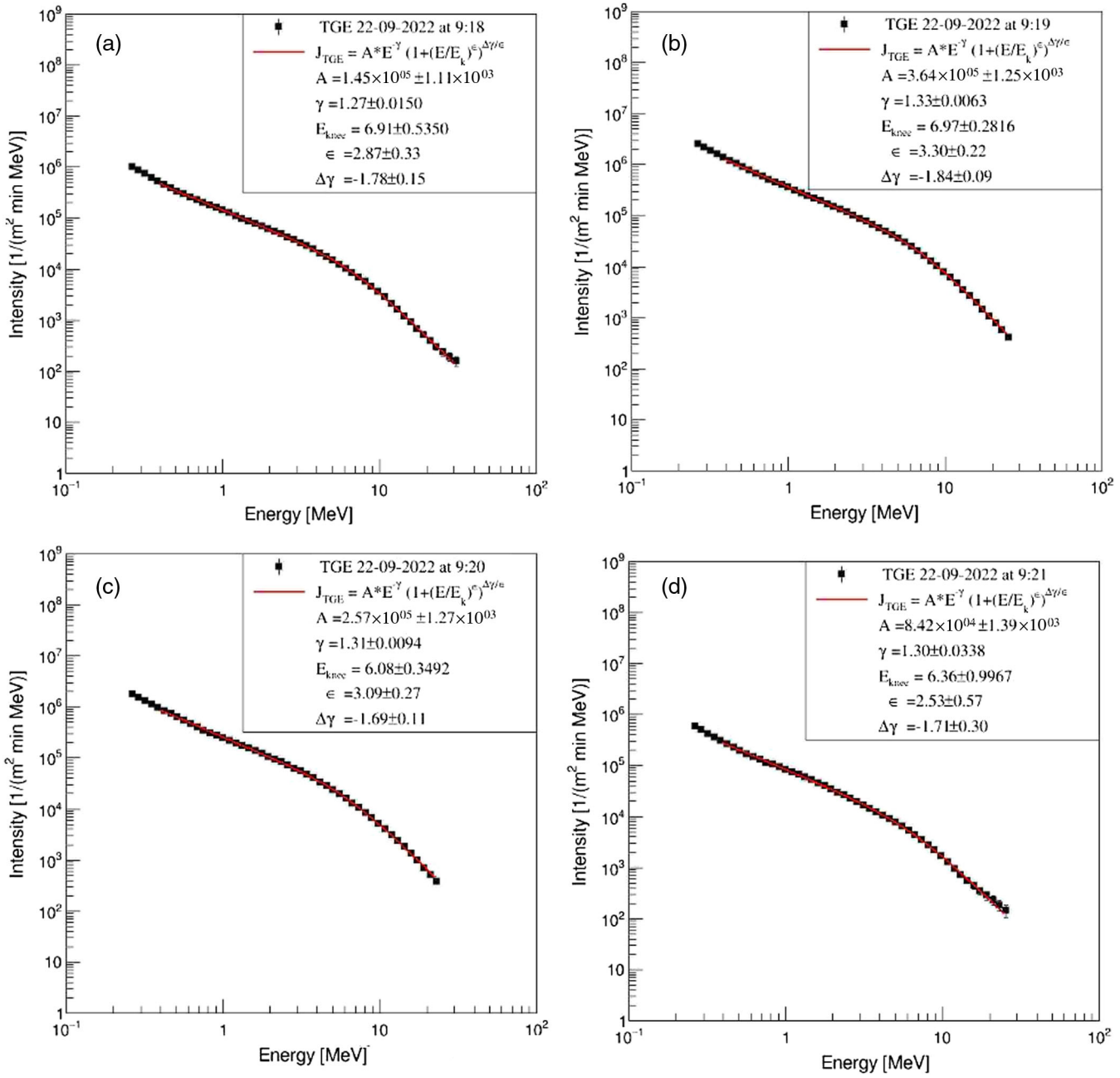

FIG. 6. TGE differential energy spectra recovered from the NaI (Tl) spectrometer. Parameters of five-parametric fit are shown in the legend in each frame.

the graupel cluster can thoroughly screen the ground from a larger main negative (MN) layer; NSEF will be positive. If the graupel cluster is small or high above the ground, it can only partially screen the NSEF sensors from MN; NSEF will be negative or change from negative to positive. Thus, the camera shots indirectly confirm the NSEF positive sign.

B. The TGE's electron and gamma ray energy spectrum recovery on 22 September 2022 at 4:22

At 4:22 and 4:27, two short TGEs occurred; see Fig. 10. Both events were very close by the amplitude of the TGE enhancement and by the lightning type that terminated them at 4:23:14.470 and 4:47:43:940. The kind of lightning was determined according to the methodology described in [10], comparing the discharges registered by two NSEF sensors on Aragats and Nor Amberd. Normal intercloud lightning flash IC+ was registered as well by the world-wide lightning location network (WWLLN, [17]) within half of a second from our detection (at 04:23:14.978). In contrast, the polarity of the NSEF was opposite (blue curve in Fig. 10) for these two TGEs. In Fig. 11, we can see that the TGE of 4:22 occurred during a deep negative electric

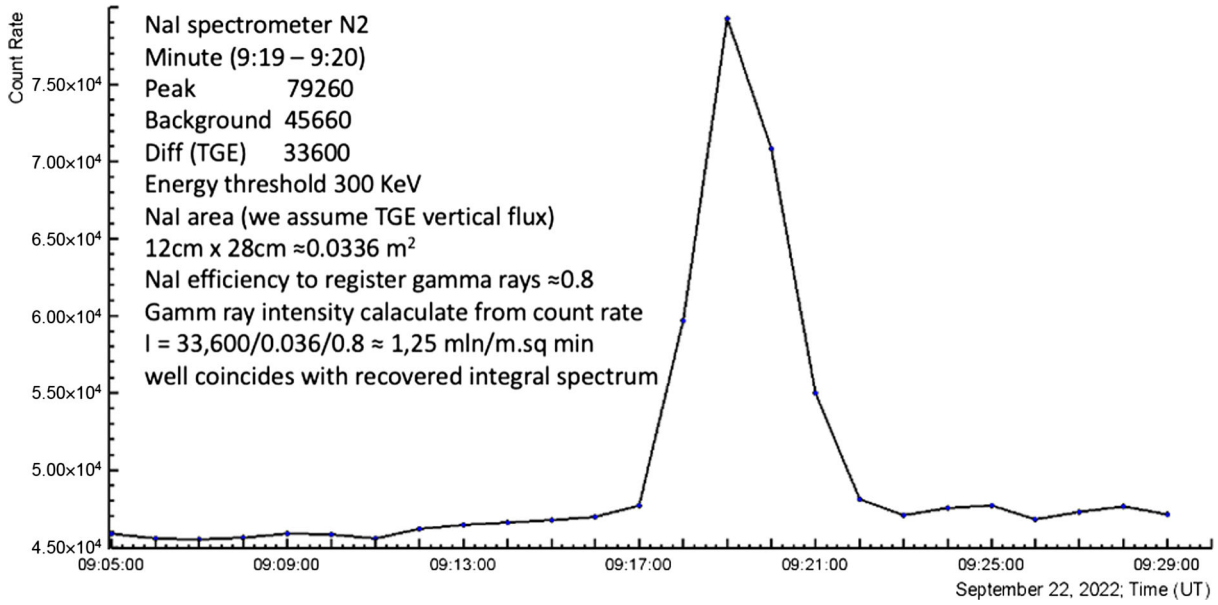

FIG. 7. Time series of 1-min count rate of NaI spectrometer N2. In the inset, we show the TGE flux calculation.

field (≈ -20 kV/m) and was terminated by a lightning flash after reaching the maximum (the flux decreases by 34% in 2 s). The TGE of 4:27 occurred during positive NSEF (+15 kV/m) and was terminated by a lightning flash at the end of the TGE development. The two scenarios of the lower dipole emergence between the main negative layer, and its mirror in the Earth and between the same main negative and LPCR were described in detail in [18].

In Fig. 11, we show zoomed versions of TGE events shown in Fig. 10, now in percent of enhancement relative to the fair-weather mean count rate. During TGE from 4:22:14 to 4:23:12, the "11" coincidence enhancement reaches ≈10%; see the green curve above the yellow line, Fig. 11(a). Thus, we can expect a sizable number of electrons. In the second 2-min-long TGE, Fig. 11(b), there is no enhancement of the "11" coincidence above the yellow line; consequently, electrons do not reach the detector.

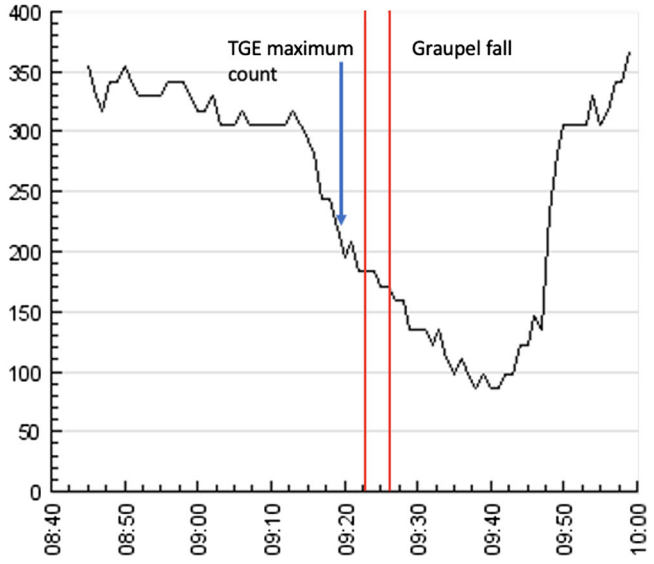

FIG. 8. Time series of distances to the cloud base. During the TGE maximum at 9:19 (denoted by a blue arrow) distance to the cloud base was ≈200 m. Red lines indicate the graupel fall (9:22–9:26).

The next step to check if TGE electrons reach the detector is examining the energy release histogram in the upper 5 cm thick scintillator; see Fig. 12. We simulate the energy release of gamma rays in the 5-cm thick scintillator using the gamma ray energy spectra recovered by "01" coincidence in the 60 cm thick "spectrometric" scintillator.

In Fig. 12, the green curve is measured energy release in the 5 cm thick scintillator.

The black curve is the gamma ray energy release histogram obtained by GEANT4 simulation using the recovered gamma ray energy spectrum and performing a full particle transport simulation through the ASNT detector. The difference between these two histograms, the red histogram, is an estimate of the electron energy release in a 5 cm thick scintillator. Recovered this way, the number of electrons (the integral of the red curve in Fig. 12) was ≈15000.

Most electrons release 6–8 MeV n the 5 cm thick scintillator (see peaks in green and red histograms), as is expected due to ≈1.8 MeV ionization losses in 1 cm of the scintillator. The registered number of electrons in the upper 5 cm scintillator is 15000; in the lower 60 cm thick, only 4100. These 4100 electrons were used in the energy spectrum recovery shown in Fig. 13. The higher than >10 MeV energy releases are due to multiple particle traversal through the scintillator. During TGE, such events are significantly enlarged compared with fair weather.

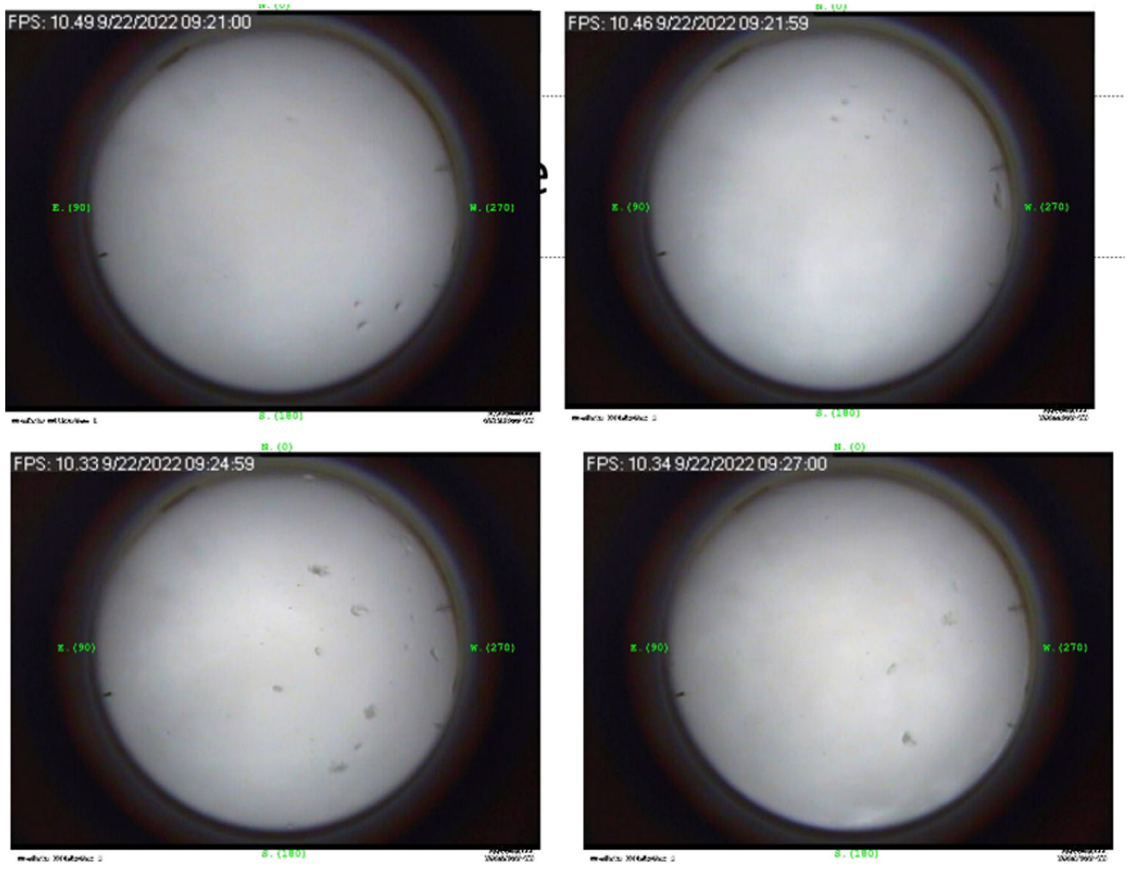

FIG. 9. The panoramic shots of the skies above Aragats just after the TGE. The specks on the photos are identified with graupel falling on the camera's glass.

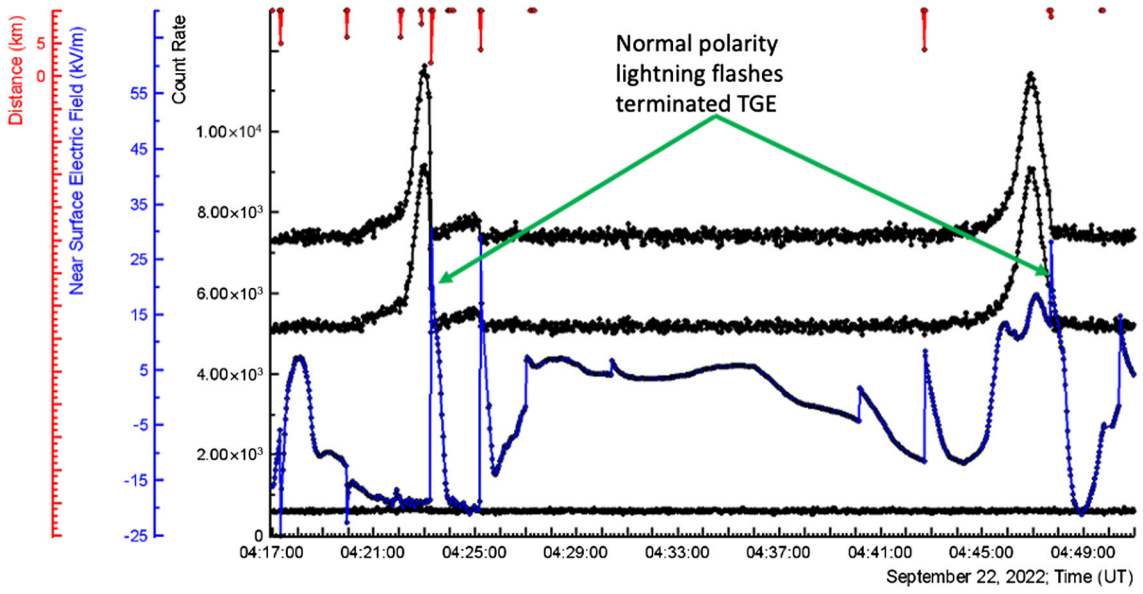

FIG. 10. Time series of count rates measured by ASNT's 60 cm thick scintillator (upper black curve), 5 cm thick scintillator (middle black curve), and "11" coincidence (lower black curve); disturbances of NSEF with abrupt increases corresponding to the lightning flashes (blue curve); distances to the lightning flash (red lines). Green arrows are directed to normal polarity lightning flashes, which terminate TGEs at 4:23:14.470 (distance to the flash 3.5 km) and 4:47:42. (distance to the flash—8.5 km).

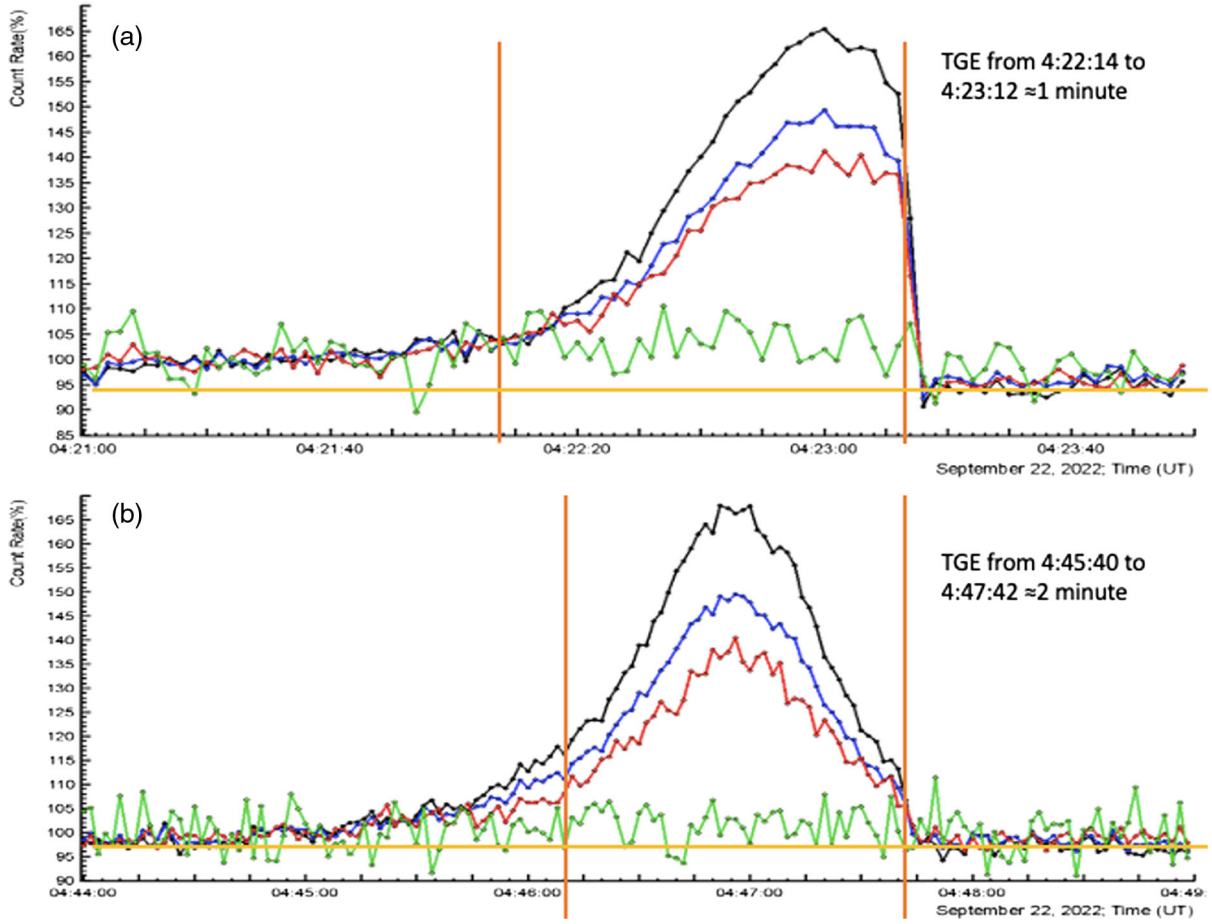

FIG. 11. (a) time series of count rates of 4:47 TGE (60 cm thick, black), with a veto to charged particles ("01" coincidence, blue), 5 cm thick (red), and primarily electrons ("11" coincidence, green); (b) the same for the TGE of 4:22. The yellow line denotes the fair-weather count rate, two magenta lines show the TGE duration.

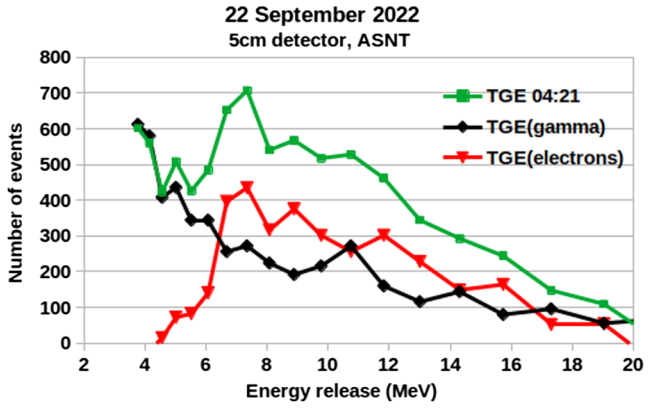

FIG. 12. Measured energy release histogram in 5 cm thick scintillator at 4:21–4:22 UT, green; histogram of the energy release of gamma rays, black; residual histogram, electron energy release, red.

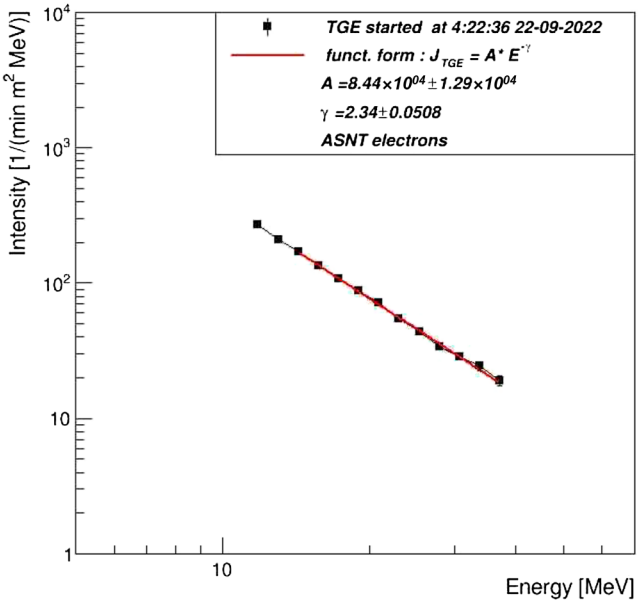

FIG. 13. TGE electrons' energy-release spectra recovered from the histograms in the ASNT's 60 cm thick scintillator.

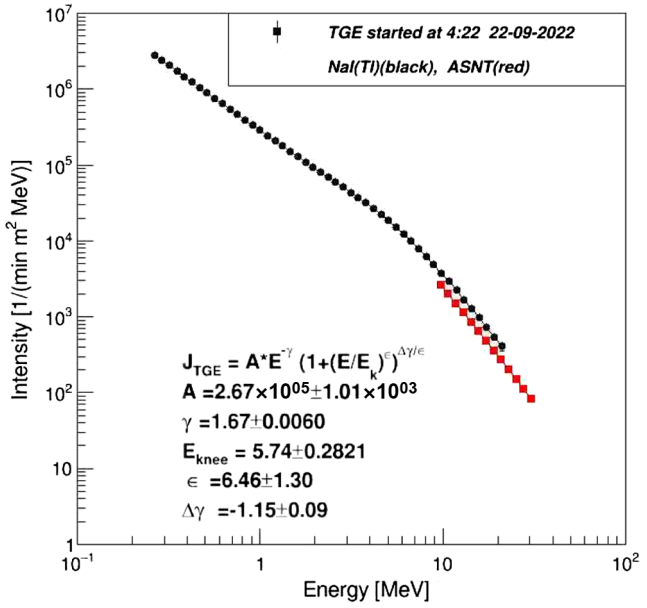

FIG. 14. TGE differential energy spectra obtained with NaI (black, energy threshold 0.3 MeV, and ASNT (red, energy threshold 10 MeV) spectrometers.

The recovery of gamma ray and electron energy spectra is performed by solving the inverse problem of cosmic rays with a detailed particle transport simulation through the detector setup, including the selection of robust *a priori* energy spectrum for calculating bin-to-bin migration (see details in [12]). In Fig. 13, we present the resulting electron differential energy spectrum. The minimum electron energy that the ASNT spectrometer can reliably recover is 10 MeV.

In Fig. 14, we compare TGE particle differential energy spectra recovered with two independent spectrometers, ASNT and NaI. ASNT spectrometer measures energy spectra with good statistics because of a 4 m^2 sensitive area; however, it misses low energy particles (below 10 MeV) due to attenuation in the substance of the massive detector. NaI spectrometer is located under the roof built with 0.6 mm tilts and can measure energy spectrum from 0.3 MeV; however, due to the small sensitive area (0.036 m^2) and relatively low electron flux, the electron spectrum can be measured only with ASNT spectrometer. After 10 MeV, both spectra coincide well.

TABLE I. Parameters of the five-parametric fit of the gamma ray energy spectra. Parameter errors are shown in Figs. 6 and 14.

Time 22/09 2022	γ_1	γ_2	$A/100,000$	E_{knee}	Sharpness
4:22	1.67	2.82	2.89	6.21	6.70
4:46	1.59	2.81	1.86	7.06	5.99
4:47	1.57	3.05	1.91	7.44	3.33
9:18	1.27	3.05	1.45	6.91	3.30
9:19	1.33	3.17	3.64	6.97	3.30
9:20	1.31	3.0	2.57	6.08	3.09
9:21	1.30	3.01	0.84	6.36	2.53

Parameters of gamma ray energy spectra measured on 22 September are summarized in Table 1. If the spectral indices after the knee (>7 MeV) are the same for TGEs occurred at 4:22, 4:47, and 9:18, the index before the knee (0.3–7 MeV) is strictly different, probably due to changing atmospheric conditions.

C. Small TGE events occurred on 22 September 2022: the LPCR emergence and contraction

The series of TGE events that occurred at 3:10–3:22 was not significant by amplitude but extended long enough to follow excursions of NSEF and corresponding changes in the particle count rates and occurrences of lightning flashes. The first TGE started during positive NSEF of +8 kV/m and was abruptly terminated ≈1 min later by an inverted intracloud flash stroked at a ≈1.5 km distance.

Attempts to start TGE afterward during negative NSEF reaching −8 kV/m at 3:12–3:16 were unsuccessful, and count rate enhancement was minimal. At 3:17–3:19, NSEF sign reversal occurred, recovering the +8 kV/m value. However, two nearby normal intracloud flashes (6.5 and 4.5 km) did not allow TGE to progress. Only after another NSEF sign reversal when the NSEF value reaches −18 kV/m does TGE restart at 3:19 and smooth finish at 3:22; see Fig. 15. Thus, we again observe TGEs both at negative and positive NSEF.

Attempts to start TGE during not large negative NSEF (−9 kV/m) were unsuccessful; only during deep negative NSEF count rate increase significantly.

During positive NSEF, an LPCR was formed, as we can see from the patterns on the glass of the panoramic camera in Fig. 16. After finishing both episodes of positive NSEF, we detect the graupel fall (3:12–3:13 and 3:18–3:20), which evidenced the decay of the LPCR sitting on graupel.

Another small TGE occurred again during the positive NSEF that reached +18 kV/m and extended from 4:57 to 5:07. The first attempt to start TGE at 4:59 was terminated by inverted polarity lightning. However, afterward, TGE restarted at 5:00 and smoothly finished at 5:05; see Fig. 17. Thus, the lower dipole was formed by the main negative layer and LPCR; and decayed with fallen graupel. The camera shots demonstrate characteristic specks of the graupel fall at 5:07–5:08, just after reversing the positive NSEF and contracting of TGE; see Fig. 18.

D. Comparison of count rates measured by STAND3 and SEVAN detectors with ones obtained from integral energy spectra recovered from ASNT

TGE energy spectra recovered by the ASNT spectrometer were checked with particle detectors operated at the Aragats station. Background count rates of the STAND3 and SEVAN detectors were calculated with EXPACS code [19], and during TGE, to the background were added

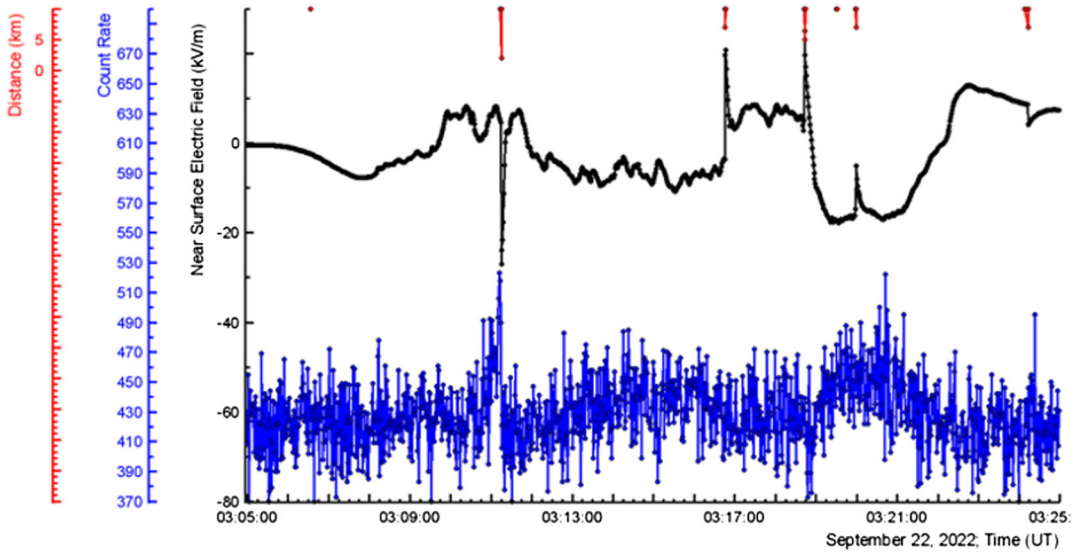

FIG. 15. Disturbances of the NSEF, black; time series of 1 s count rates of STAND1 plastic scintillator of 1 m^2 area and 1 cm thickness, blue; distances to lightning flashes, red.

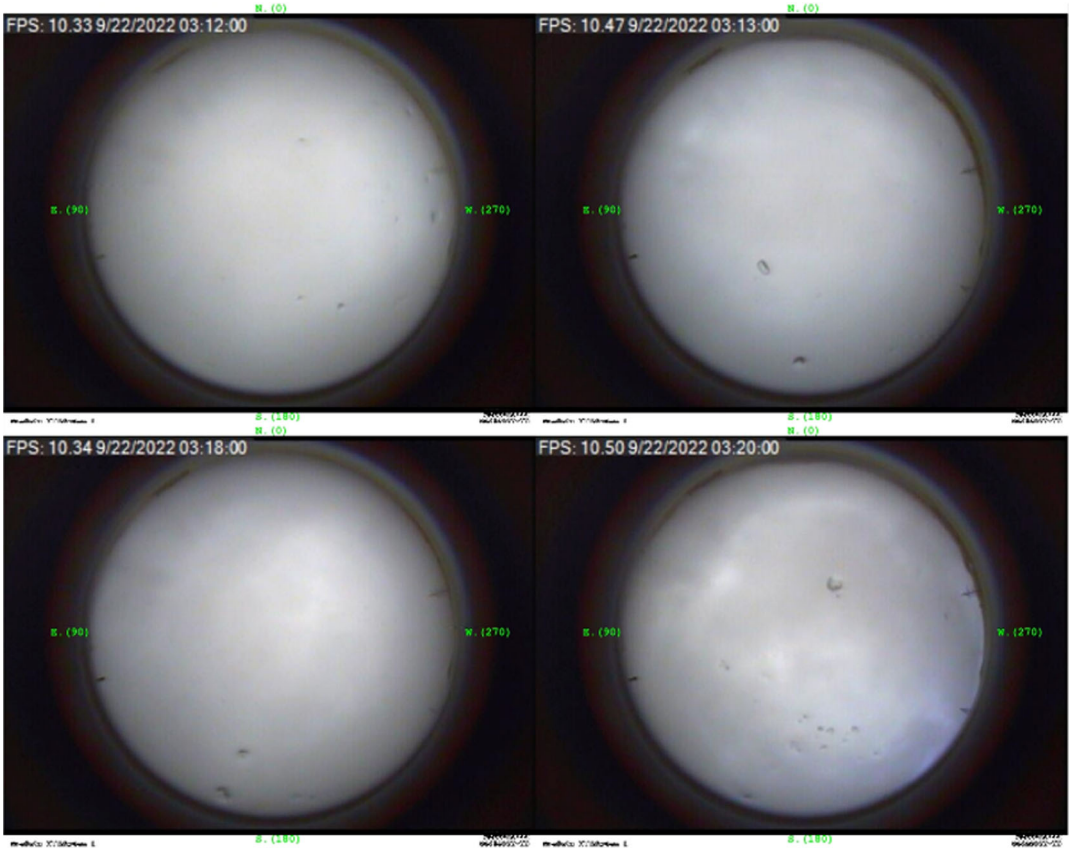

FIG. 16. Shots of the panoramic camera showing characteristic specks on the glass, which identified the graupel fall.

the TGE spectra recovered by ASNT (presented in the previous sections). Background and TGE spectra were tracked through particle detectors with the GEANT4 code [20]. The vertically stacked STAND3 detector was described above (in the discussion of Fig. 2). The SEVAN detector [21], located 20 m from ASNT and 100 m from STAND3, consists of standard slabs of $50 \times 50 \times 5$ cm^3 plastic scintillators. Between two identical assemblies of $100 \times 100 \times 5$ cm^3 scintillators (four standard slabs) are located two $100 \times 100 \times 4.5$ cm^3 lead absorbers and a

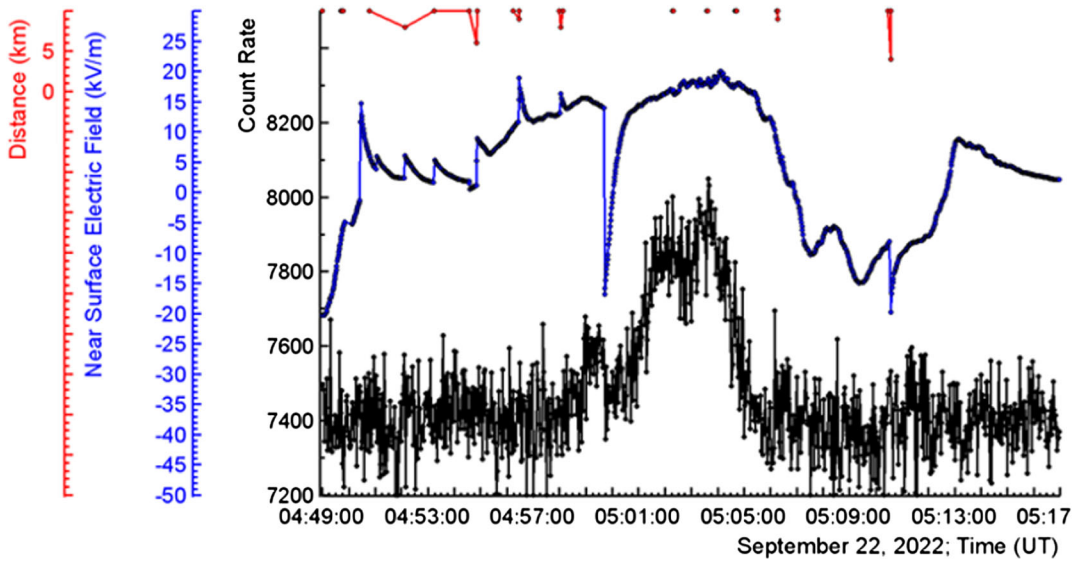

FIG. 17. Time series of 2 s count rates of ASNT scintillator of 4 m^2 area and 60 cm thickness, black; disturbances of the NSEF, blue; distances to lightning flashes, red.

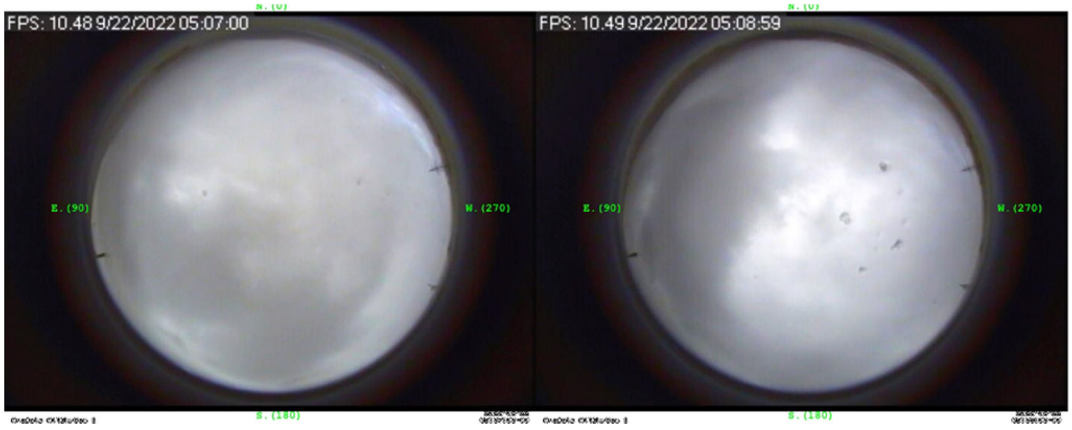

FIG. 18. Shots of the panoramic camera showing characteristic specks on the glass, which were identified with graupel fall.

thick $50 \times 50 \times 25$ cm^3 scintillator stack (5 standard slabs). Lights capture cones and photomultipliers (PMTs) are located on the detector's top, bottom, and intermediate layers. In Figs. 19–21, we compare measured and simulated count rates for the largest TGEs observed on 22 September.

Figures 19–21 show a good agreement between count rates calculated from the ASNT spectra and measured by STAND3 and SEVAN detectors, proving the correctness of electron and gamma ray energy spectra recovery with ASNT.

E. Correlation analysis of the TGE particle fluxes: Getting insight into the atmospheric electric field

Thundercloud charges and emerging atmospheric electric fields are the most challenging processes for measuring and modeling. The relation of cloud electrification and particle fluxes emerging in the cloud and traversing it remains at the top of high-energy physics in the atmosphere (HEPA) research. The interactions with solar radiation and cosmic ray fluxes, atmospheric discharges, and winds lead to the highly volatile behavior of the atmospheric electric fields. Electric charge in the atmosphere remains quasistatic at different altitudes for brief periods (of the order of milliseconds), and there is no possibility of obtaining an analytical solution to the electrodynamic of the charged cloud. The phenomenological approach is the only one allowing investigation of the correlations of the emerging electric fields and particle fluxes on a minute timescale. The atmospheric electric fields originating TGEs can be researched by measuring the energy spectra of TGE particles. By registering TGE particle fluxes, we can relate them to the atmospheric conditions that are more-or-less stable during the TGE development.

The most intense TGEs are usually abruptly terminated by lightning flashes; nonetheless, their duration rates from a few to tens of minutes [22]. We developed the particle

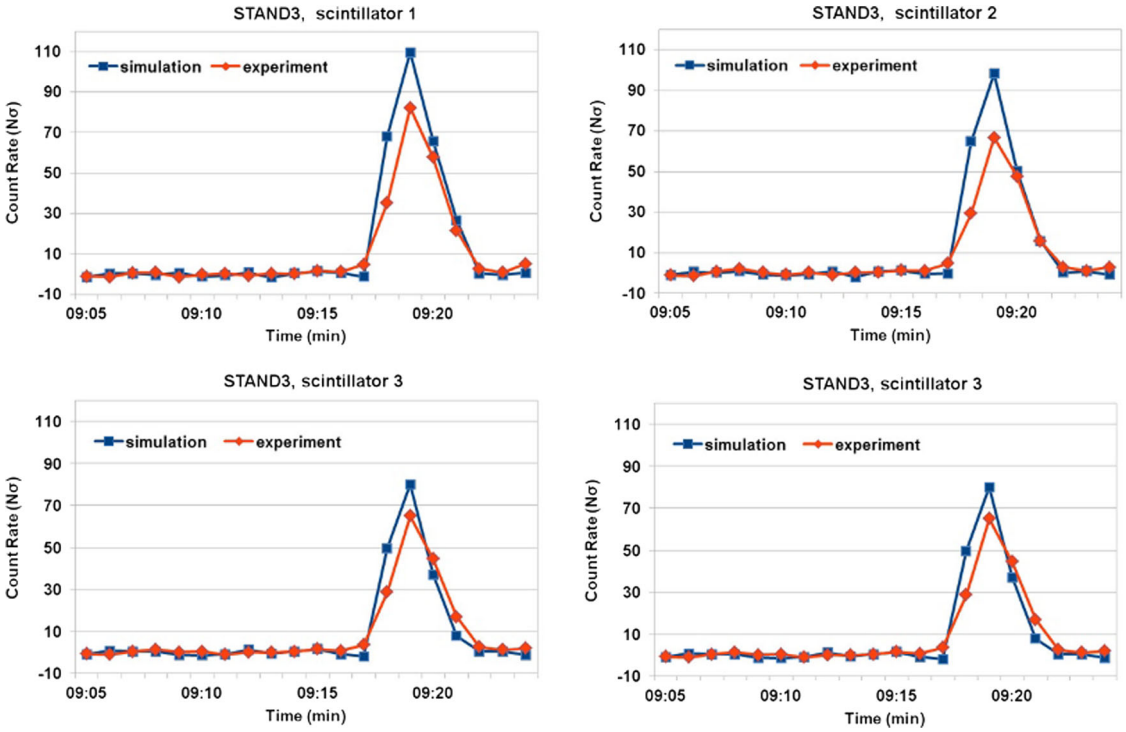

FIG. 19. Comparison of count rates measured by four stacked scintillators of STAND3 detector with calculated ones recovered by ASNT (minutes from 9:17 to 9:21).

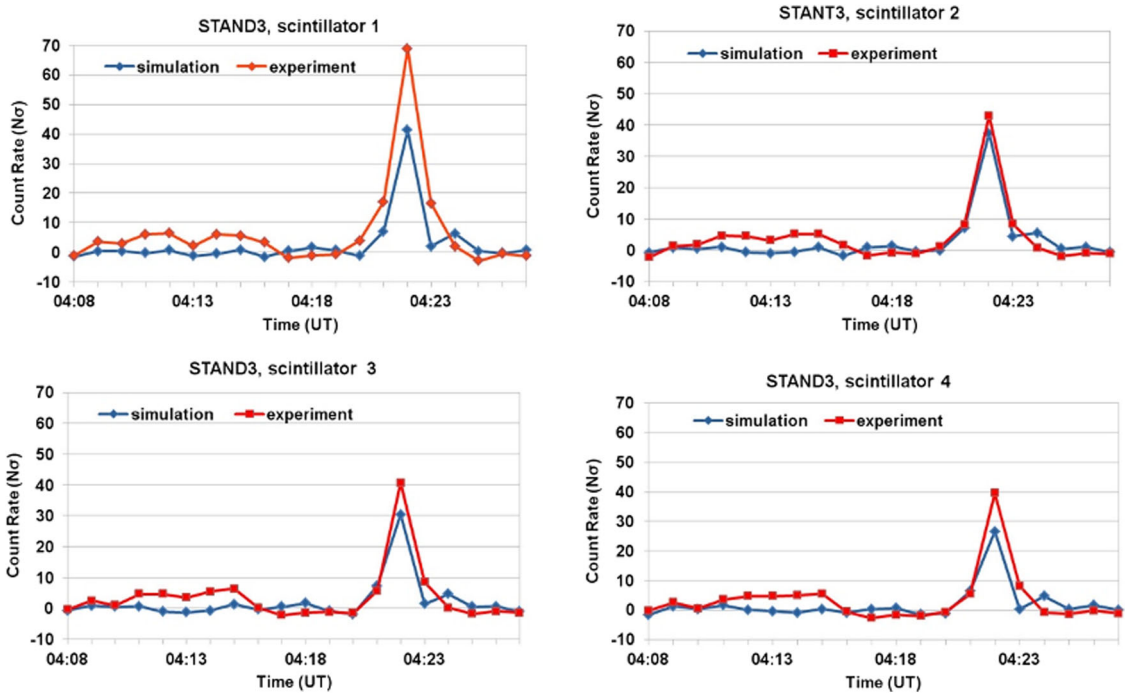

FIG. 20. Comparison of count rates measured by four stacked scintillators of STAND3 detector with calculated ones recovered by ASNT (minutes from 4:21–4:23).

detector network STAND1 synchronized with EFM 100 electric mills to understand how the electric fields change during TGE [23]. The EFM 100 sensors are operational at distances up to 33 km and estimate the distance to the lightning flash with an accuracy of ≈1.5 km. The network of STAND1 particle detectors (see Fig. 22) comprises three units of stacked plastic scintillators 1 cm thick, 1 m^2 sensitive-area scintillators each. The three National

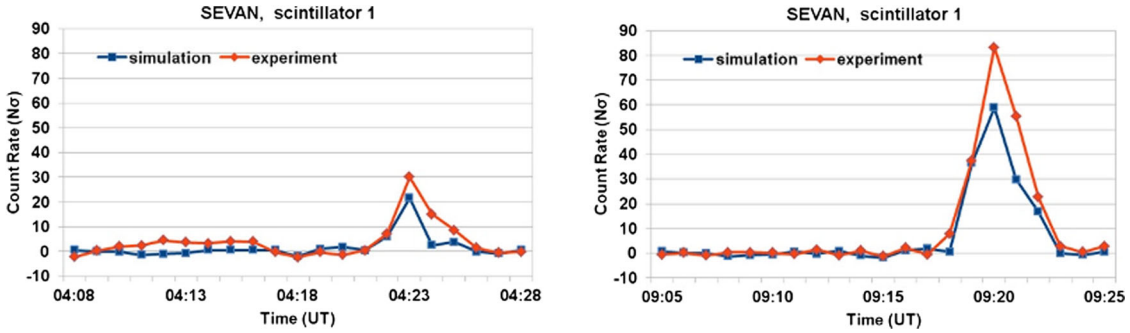

FIG. 21. Comparison of count rates measured by upper scintillator of SEVAN detector with calculated ones recovered by ASNT.

Instrument's MyRio boards generate an output signal containing each site's scintillator's count rates and NSEF measurements. The fast, synchronized data acquisition (FSDAQ, [24]) provides particle fluxes and NSEF disturbances registration with millisecond accuracy.

To investigate the correlations between particle fluxes and NSEF disturbances, we developed in the data analysis platform ADEI statistical methods for the visualization of time series and calculating the "delayed" correlations obtained by moving the time series relative to each other.

In Figs. 23(a) and 23(b), we show 1-s time series of STAND1 network count rates for the two largest TGEs occurred during positive NSEF. STAND1 units on the highland near MAKET and SKL experimental halls (blue and red curves) demonstrate coherent TGE rise and decay.

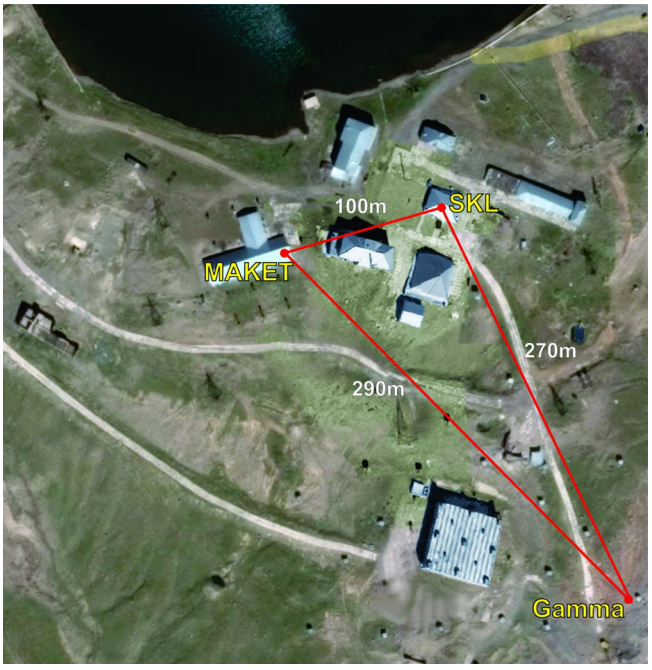

FIG. 22. STAND1 detector network. Each of the three units comprises vertically stacked three 1 cm thick and 1 m^2 area plastic scintillators and the same area stand-alone 3 cm thick plastic scintillator.

For the unit located 20 m lower and 300 m distance from the MAKET hall (black curve), which is opened to Ararat Valley, electric field conditions are slightly different, and the maximum flux was reached several seconds earlier. Nonetheless, the STAND1 network demonstrates that the electric field in the cloud above was stable for several minutes providing appropriate conditions for developing the electron-gamma ray avalanche. In this way, TGE detection allows fixing minutes-long periods when a strong intracloud electric field reaches 2.0 kV/cm 1–2 km vertically (the primary condition of the TGE origination).

Thus, for the TGE that started at 4:45:20 [Fig. 23(a)], there were ≈3 min more-or-less smoothly changing the intracloud electric field, and for TGE, that began at 9:17:30–≈4 min. As mentioned above, TGE occurrence poses very stringent conditions on the accelerating electric field, which remain more-or-less stable during particle flux enhancement and consequent smooth decay. It allows us to investigate the correlation of the atmospheric electric field, which accelerates electrons with the intensity of the particle flux. In Fig. 24, we show the results of the correlation analysis made for the STAND1 units nearby MAKET 24(a) and SKAL 24(b) experimental halls for the TGE started at 4:45:20. As we can see, with the growing NSEF, the particle flux correspondingly increases, and when NSEF declines particle flux coherently declines. We calculate correlation coefficients between particle fluxes and NSEFs (R) separately for TGE's ascending and descending phases, which are very significant. Figures 25(a) and 25(b) show the same relations for the TGE started at 9:17:30. The similarity of the correlation patterns for the distributed particle detectors demonstrates that the atmospheric electric field can be relatively stable for up to 10 min at distances ≈ of 300 m, sustaining conditions for electron acceleration. Only such a "frozen" static state of the atmospheric electric field allows TGE origination.

F. Discussion and conclusions

Research of atmospheric electron accelerators requires the 24/7 operation of advanced particle detectors. Free electrons from the ambient population of cosmic rays born

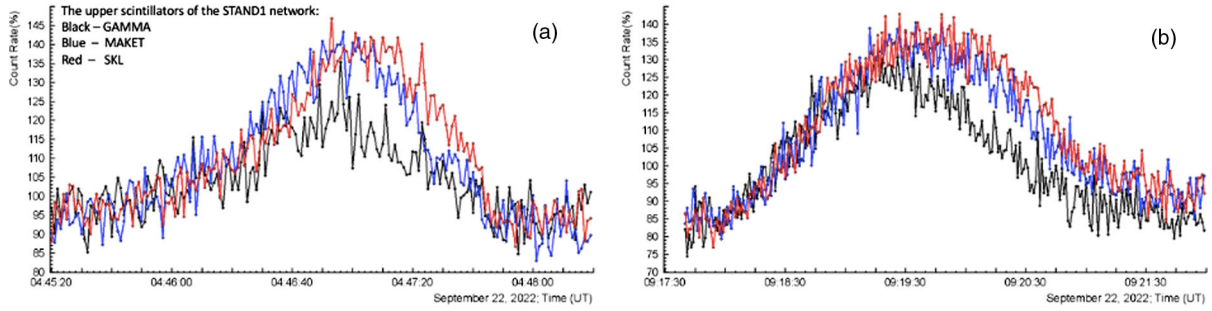

FIG. 23. Count rates (relative to fair weather) of three scintillators of STAND1 network located in nodes of a triangle with sides 100, 250, and 300 m.

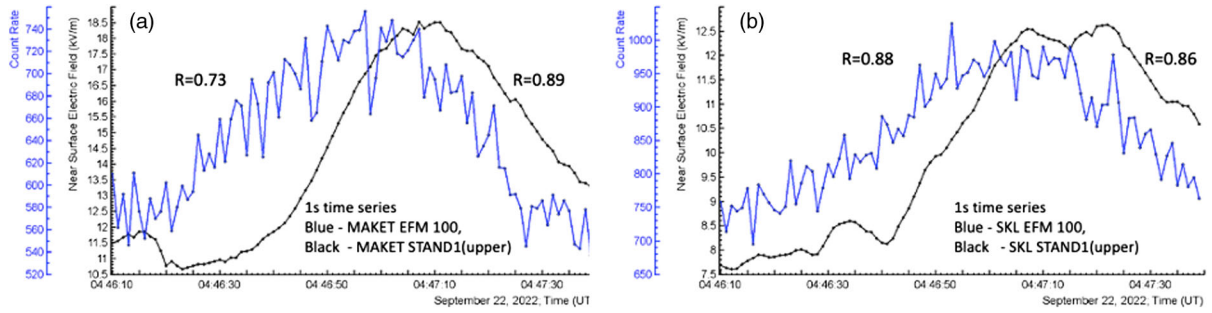

FIG. 24. 1-s time series of NESF disturbances and TGE fluxes measured by an EFM 100 electric mill and STAND1 upper scintillator outside the experimental halls of MAKET and SKL. Correlation coefficients (R) were calculated separately for the ascending and descending TGE phases.

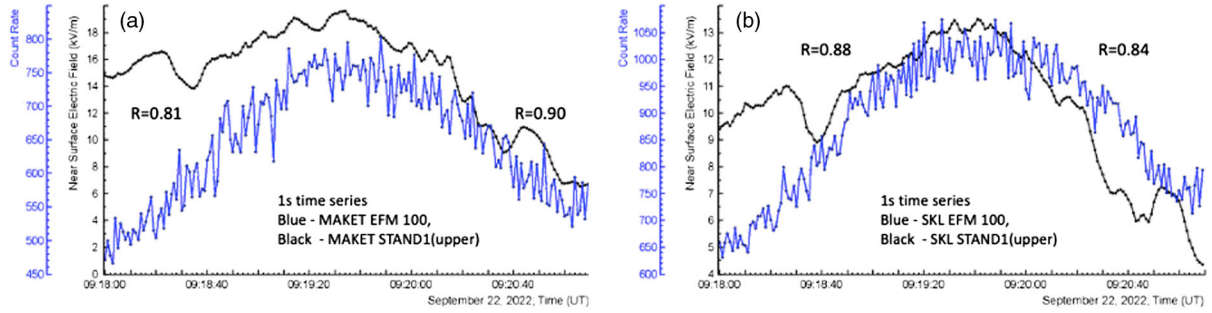

FIG. 25. 1-s time series of NESF disturbances and TGE fluxes measured by an EFM 100 electric mill and STAND1 upper scintillator outside the experimental halls of MAKET and SKL. Correlation coefficients (R) were calculated separately for the ascending and descending TGE phases.

in the strong interactions of the galactic hadrons or gamma rays with atmospheric atoms are modulated by the strong electric field of the thunderous atmosphere.

On September 22, 2022, various TGE events occurred, each under a specific condition. TGEs occurred during positive NSEF, negative NSEF, and the electric field sign reversal. Correspondingly, a lower dipole was formed by the main negative (MN) charge region in the middle of the cloud and its mirror in the earth or/and the same MN and LPCR. By monitoring the NSEF and graupel fall, we demonstrate that LPCR is a transient layer sitting on graupel and disappears with graupel fall.

The TGE energy spectrum measured at minutes 9:19–9:20 was extraordinarily intensive. During the most intense minute, TGE flux reaches ≈1.25 million particles (with energies exceeding 0.3 MeV) per minute per m^2, with the highest energy reaching 70 MeV. The radon progeny gamma radiation governs the relatively soft energy spectra at low energies. After the knee, the spectra became hard and continued to energies up to 70 MeV. However, at the highest energies, the contribution of the MOS process [25], negligible at lower energies, becomes essential. Thus, the genuine maximum energy of the TGE particles hardly exceeds 50 MeV.

We estimate the electric field strength and extension by measuring the energy spectra of TGE electrons and gamma rays [26]. Using particle fluxes measured by the distributed STAND1 network, we present the correlations between particle fluxes and near-surface electric fields. The enhancing intracloud electric field controls the enhancement of TGE flux. When NSEF declines, particle flux diminishes. TGEs occurring during positive electric fields prolonged for ten min, and the atmospheric electric field that originated them smoothly enhanced and decreased. Thus, during TGEs, a quasi-static charged structure remains stable for minutes. The smooth changes of accelerating electric field we relate to moving graupel cluster.

During negative NESF at 4:22, TGE was abruptly terminated by a lightning flash just after the maximum of its development. Possibly at the maximum electron flux, the lightning leader found the path and lowered voltage in the cloud stopping the TGE. As it was normal polarity intercloud discharge, we can speculate that a symmetric particle flux was developing in the upper dipole between the main negative and positive regions.

Thus, lightning flashes on September 22, 2022, abruptly terminate TGEs in the beginning, at the maximum, and at the decaying of the particle flux. It means that RREA/TGE process precedes the lightning flash; i.e., it is a precursor. Sure, we did not observe the lightning initiation process. We have no developed model of lightning leaders or streamers using the ionized path opened by an RREA for their development. Nonetheless, by measuring both lightning flashes and particle fluxes, we obtained definite relations between both

(i) About 70% of TGEs are abruptly interrupted by a lightning flash.
(ii) Lightning terminates TGE in the initial stage, in the maximum, and at the decaying stage.
(iii) The distance to the flash is 1–10 km.
(iv) The duration of the TGEs, which are terminated by lightning, is usually 1–2 min, not larger than 5 min.
(v) After the lightning flash, the maximum energy of TGE particles shrinks to 3 MeV, the runaway process stops, and only radon progeny gamma radiation remains till the complete decay of long-lived ^{214}Pb and ^{214}Bi isotopes.
(vi) Usually, after termination, the particle flux again rises till another lightning terminates it, and so on up to 5 times.
(vii) If lightning sensors do not register any atmospheric discharge within 10 km, TGE smoothly finished with a bell-like shape prolonging up to 20 min.

Evidence from other experiments also confirms that RREA precedes lightning flashes.

(i) Balloon and aircraft detectors usually observe TGE abruptly terminated by the lightning flash; see references in [26].
(ii) The group from Langmuir Laboratory in central New Mexico, after examining 23 thunderstorm soundings, suggests that lightning occurs whenever the electric field exceeds the critical field [27]. The same group observed during balloon flights on 3 July 1999 the maximal field of 1.86 kV/cm (130% of the threshold for starting a runaway process) at 5.77 km altitude just before nearby lightning flashes [28].

TGEs and lightning flashes depend on the strength of the atmospheric electric field and occur when the critical value of this strength is reached. We know the critical value for RREA initiation for each height (air density); for the lightning initiation, the critical value should be larger than the critical value for RREA because TGEs preceded lightning flashes that terminate them. Or atmospheric conditions after the RREA changes in a way to make the path for the lightning leader easier. From the TGE-lightning time sequence measured on Aragats during the last 15 years, we can assume that strong electric fields initiate intense electron-gamma ray avalanches and, afterward—lightning flashes when RREA electrons do enough ionization in the atmosphere to make more accessible the path for a lightning leader.

Data availability statement: The data supporting this study's findings are available at the following [29].

ACKNOWLEDGMENTS

We thank the staff of the Aragats Space Environmental Center for the uninterruptable operation of all particle detectors and field meters. The authors acknowledge the support of the Science Committee of the Republic of Armenia (Research Project No. 21AG-1C012) in the modernization of the technical infrastructure of high-altitude stations.

[1] A. Chilingarian, A. Daryan, K. Arakelyan, A. Hovhannisyan, B. Mailyan, L. Melkumyan, G. Hovsepyan, S. Chilingaryan, A. Reymers, and L. Vanyan, Ground-based observations of thunderstorm-correlated fluxes of high-energy electrons, gamma rays, and neutrons, Phys. Rev. D **82**, 043009 (2010).
[2] A. Chilingarian, G. Hovsepyan, and A. Hovhannisyan, Particle bursts from thunderclouds: Natural particle accelerators above our heads, Phys. Rev. D **83**, 062001 (2011).
[3] J. Chum, R. Langer, J. Baše, M. Kollárik, I. Strhárský, G. Diendorfer, and J. Rusz, Significant enhancements of

secondary cosmic rays and electric field at high mountain peak during thunderstorms, Earth Planets Space **72**, 28 (2020).
[4] A. V. Gurevich, G. M. Milikh, and R. Roussel-Dupre, Runaway electron mechanism of air breakdown and preconditioning during a thunderstorm, Phys. Lett. A **165**, 463 (1992).
[5] A. Chilingarian, G. Hovsepyan, E. Svechnikova, and M. Zazyan, Electrical structure of the thundercloud and operation of the electron accelerator inside it, Astropart. Phys. **132**, 102615 (2021).
[6] A. Chilingarian and H. Mkrtchyan, Role of the lower positive charge region (LPCR) in the initiation of the thunderstorm ground enhancements (TGEs), Phys. Rev. D **86**, 072003 (2012).
[7] J. Kuettner, The electrical and meteorological conditions inside thunderclouds, J. Meteorol. **7**, 322 (1950).
[8] A. Chilingarian, G. Hovsepyan, D. Aslanyan, T. Karapetyan, Y. Khanikyanc, L. Kozliner, B. Sargsyan, S. Soghomonyan, S. Chilingaryan, D. Pokhsraryan, and M. Zazyan, Thunderstorm ground enhancements: Multivariate analysis of 12 years of observations, Phys. Rev. D **106**, 082004 (2022).
[9] S. Soghomonyan, A. Chilingarian, and Y. Khanikyants, Dataset for thunderstorm ground enhancements terminated by lightning discharges, Mendeley Data, V1 (2021), 10.17632/p25bb7jrfp.1, https://data.mendeley.com/datasets/p25bb7jrfp/1.
[10] A. Chilingarian, Y. Khanikyants, V. A. Rakov, and S. Soghomonyan, Termination of thunderstorm-related bursts of energetic radiation and particles by inverted intracloud and hybrid lightning discharges, Atmos. Res. **233**, 104713 (2020).
[11] A. Chilingarian, G. Hovsepyan, T. Karapetyan, Y. Khanykyanc, D. Pokhsraryan, B. Sargsyan, S. Chilingaryan, and S. Soghomonyan, Multi-messenger observations of thunderstorm-related bursts of cosmic rays, J. Instrum. **17**, P07022 (2022).
[12] A. Chilingarian, G. Hovsepyan, T. Karapetyan, B. Sarsyan, and S. Chilingaryan, Measurements of energy spectra of relativistic electrons and gamma-rays avalanches developed in the thunderous atmosphere with Aragats Solar Neutron Telescope, J. Instrum. **17**, P03002 (2022).
[13] A. Chilingarian, G. Gharagyozyan, S. Ghazaryan, G. Hovsepyan, E. Mamidjanyan, L. Melkumyan, V. Romakhin, A. Vardanyan, and S. Sokhoyan, Study of extensive air showers and primary energy spectra by MAKET-ANI detector on mountain aragats, Astropart. Phys. **28**, 58 (2007).
[14] S. Ter-Antonyan and L. Haroyan, About EAS size spectra and primary energy spectra in the knee region, arXiv: hep-ex/0003006.
[15] A. Chilingarian, G. Hovsepyan, and B. Sargsyan, Circulation of Radon progeny in the terrestrial atmosphere during thunderstorms, Geophys. Res. Lett. **47**, e2020GL091155 (2020).
[16] A. Chilingarian, G. Hovsepyan, G. Karapetyan, and M. Zazyan, Stopping muon effect and estimation of the intracloud electric field, Astropart. Phys. **124**, 102505 (2021).
[17] C. J. Rodger, S. Werner, J. B. Brundell, E. H. Lay, N. R. Thomson, R. H. Holzworth, and R. L. Dowden, Detection efficiency of the VLF World-Wide Lightning Location Network (WWLLN): Initial case study, Ann. Geophys. **24**, 3197 (2006).
[18] A. Chilingarian, G. Hovsepyan, T. Karapetyan, B. Sargsyan, and M. Zazyan, Development of the relativistic runaway avalanches in the lower atmosphere above mountain altitudes, Europhys. Lett. **139**, 50001 (2022).
[19] T. Sato, Analytical model for estimating terrestrial cosmic ray fluxes' zenith angle dependence, PLoS One **11**, e0160390 (2016).
[20] S. Agostinelly, J. Allison, A. Amako *et al.*, GEANT4—A simulation toolkit, Nucl. Instrum. Methods Phys. Res., Sect. A **506**, 250 (2003).
[21] A. Chilingarian, V. Babayan, T. Karapetyan, B. Mailyan, B. Sargsyan, and M. Zazyan, The SEVAN worldwide network of particle detectors: 10 years of operation, Adv. Space Res. **61**, 2680 (2018).
[22] A. Chilingarian, S. Chilingaryan, T. Karapetyan, Lev Kozliner, Yeghia Khanikyants, Gagik Hovsepyan, David Pokhsraryan, and Suren Soghomonyan, On the initiation of lightning in thunderclouds, Sci. Rep. **7**, 1371 (2017).
[23] D. Pokhsraryan, Fast data acquisition system based on NI-myRio board with GPS time stamping capabilities for atmospheric electricity research, in *Proceedings of the TEPA Symposium, Nor Amberd, Armenia, 5–9 October 2015* (Tigran Mets, Yerevan, Armenia, 2016), p. 23.
[24] A. Chilingarian, G. Hovsepyan, T. Karapetyan, B. Sargsyan, and E. Svechnikova, Transient luminous events in the lower part of the atmosphere originated in the peripheral regions of a thunderstorm, Universe **8**, 412 (2022).
[25] A. Chilingarian, B. Mailyan, and L. Vanyan, Recovering of the energy spectra of electrons and gamma rays coming from the thunderclouds, Atmos. Res. **114–115**, 1 (2012).
[26] A. Chilingarian, G. Hovsepyan, D. Aslanyan, T. Karapetyan, Y. Khanikyanc, L. Kozliner, D. Pokhsraryan, B. Sargsyan, S. Soghomonyan, S. Chilingaryan, and M. Zazyan, Thunderstorm ground enhancements: Multivariate analysis of 12 years of observations, Phys. Rev. D **106**, 082004 (2022).
[27] T. C. Marshall, M. P. McCarthy, and W. D. Rust, Electric field magnitudes and lightning initiation in thunderstorms, J. Geophys. Res. **100**, 7097 (1995).
[28] M. Stolzenburg, T. C. Marshall, W. D. Rust, E. Bruning, D. R. MacGorman, and T. Hamlin, Electric field values observed near lightning flash initiations, Geophys. Res. Lett. **34**, L04804 (2007).
[29] http://adei.crd.yerphi.am/.